Composition-dependent magnetic properties of $BiFeO_3$-$BaTiO_3$ solid solution nanostructures

Tae-Jin Park,[1,*] Georgia C. Papaefthymiou,[2,†] Arthur J. Viescas,[2] Yongjae Lee,[3] Hongjun Zhou,[1,‡] and Stanislaus S. Wong[1,4,†]

[1]*Department of Chemistry, State University of New York at Stony Brook, Stony Brook, New York 11794-3400, USA*

[2]*Department of Physics, Mendel Hall, Villanova University, 800 Lancaster Avenue, Villanova, Pennsylvania 19085, USA*

[3]*Department of Earth System Sciences, Yonsei University, Seoul 120749, Korea*

[4]*Condensed Matter Physics and Materials Sciences Department, Brookhaven National Laboratory, Building 480, Upton, New York 11973, USA*

(Received 6 January 2010; revised manuscript received 6 July 2010; published 29 July 2010)

We report on the Mössbauer spectra and magnetization properties of single-crystalline $(BiFeO_3)_x$-$(BaTiO_3)_{1-x}$ solid solution nanostructures in the form of nanocubes, measuring approximately 150 to 200 nm on a side, prepared by a molten salt solid-state reaction method in the compositional range wherein $0.5 \leq x \leq 1$. Powder x-ray diffraction (XRD) and monochromatic synchrotron XRD studies indicate products of high purity, which undergo gradual, well-controlled structural transformations from rhombohedral to tetragonal structures with decreasing "x." For all solid solution products, room-temperature magnetization studies exhibit hysteretic behavior with remnant magnetization values of $M_r \geq 0.32$ emu/g, indicating that the latent magnetization locked within the toroidal spin structure of $BiFeO_3$ has been released. Room-temperature Mössbauer spectra show composition-dependent characteristics with decreasing magnetic hyperfine field values and increasing absorption linewidths due to a decrease in the magnetic exchange interaction strength with decreasing x. For the lowest $x=0.5$ composition studied, the Mössbauer spectra show paramagnetic behavior, indicating a Néel temperature for this composition below 300 K. However, room-temperature magnetization studies with applied fields of up to 50 kOe show hysteretic behavior for all compositions, including the $x=0.5$ composition, presumably due to field-induced ordering. Furthermore, hysteresis loops for all compositions exhibit smaller coercivities at 10 K than at 300 K, an observation that may suggest the presence of magnetoelectric coupling in these systems.

DOI: 10.1103/PhysRevB.82.024431 PACS number(s): 75.50.Tt, 75.75.−c

I. INTRODUCTION

Ferroelectricity has been predicted and observed in perovskite-structure oxides because they possess unit-cell structural characteristics that can support deformations, which thereby lead to the appearance of permanent electric polarization.[1,2] The rare occurrence of the coexistence of ferroelectric and ferromagnetic orders[3] is believed to arise from the fact that the former requires empty d orbitals to allow cation off-center displacement leading to ferroelectricity while the latter necessitates incomplete d-orbital electronic occupation leading to ferromagnetism.

Among the perovskite oxides, $BiFeO_3$ is known to possess both types of long-range order. Specifically, it is ferroelectric below 1110 K and antiferromagnetic below 643 K.[4] In this system, magnetic order arises from the d^5-electronic configuration of the Fe^{3+} B-site cation with five unpaired spin electrons, rendering an effective local iron magnetic moment of $\sim 5.9\mu_B$ while ferroelectric order is suspected to arise from the stereochemical activity of the Bi^{3+} A-site cation with $6s$ lone pair electrons.[5–7] Neutron-scattering experiments[8,9] have established that superexchange interactions produce a canted antiferromagnetic order, where the spin-up and spin-down sublattices are not strictly antiparallel, thereby leading to weak ferromagnetism. In the bulk, however, the resulting magnetic moment shows a superimposed spiral ordering associated with a period length of 62 nm, rendering $BiFeO_3$ nonmagnetic. Many current investigations seek to suppress the spiral spin structure in an effort to release the inherent magnetization of this canted antiferromagnet and consequently improve its multiferroic properties. The spiral spin structure is known to be destroyed by factors including (a) the application of intense external magnetic fields ≥ 180 kOe,[10–12] releasing a magnetic moment of ~ 0.30 emu/g, (b) the application of external stress or interfacial strain often encountered in two-phase systems, such as thin-film heterostructures or mixtures of grains,[1] (c) the action of finite-size effects in nanophase bismuth ferrite,[13] and (d) the imposition of structural modifications or deformations introduced by cation substitutions or doping, as we discuss in greater detail below.

In our recent studies, we have focused on the synthesis of pure, single crystalline, nanosized structures of $BiFeO_3$ with the goal of producing systems with enhanced multiferroic properties. Three distinct facts motivate our approach: (a) single crystallinity eliminates grain boundaries where defects, such as Fe^{2+}, are known to accumulate, leading to reduced resistivity and inferior ferroelectric properties, (b) finite-sized effects at the nanoscale destroy the spiral spin structure associated with the bulk, releasing the latent, inherent magnetization, and (c) uncompensated spins at the surface of the nanoparticles further increase their net magnetization.

We have recently reported[13] on the enhancement of the magnetic properties in pure, single-crystalline $BiFeO_3$ nanoparticles with edge lengths ranging from 245 down to 14 nm, which span a range of particle sizes both larger than as well as smaller than the cycloidal spin wavelength of 62 nm. Herein, we report on a similar enhancement of magnetic properties in nanocubes measuring about 150–200 nm on a side brought about by rational structural modifications induced in stoichiometric, single-crystalline solid solutions of $(BiFeO_3)_x$-$(BaTiO_3)_{1-x}$ wherein $0.5 \leq x \leq 1$. Furthermore, we present experimental evidence suggestive of the presence of

magnetoelectric coupling in these solid solution nanostructures.

In practice, the incorporation of bulk multiferroic $BiFeO_3$ materials into practical devices, such as either piezoelectric or magnetoelectric functional components, has been hindered by the low value of polarization or dielectric constant at room temperature and by intrinsic leakage-current problems that lead to low electrical resistivity.[14,15] In recent years, there has been a parallel, multipronged effort to address these physical property limitations through directed, rational synthesis of stoichiometrically pure $BiFeO_3$ nanomaterials,[13] and the introduction of structural modifications by doping in order to perturb the spiral spin structure and improve the magnetic properties.[16–27] For example, the highest values of the spontaneous magnetization observed have been noted for rare-earth ion doped samples due to strong contributions from the magnetic moments of the rare-earth ions to the net magnetization. For other dopants, an increase in the radius of the *A*-site ion can lead to effective suppression of the spiral spin structure of $BiFeO_3$, thereby resulting in the appearance of net magnetization.[28]

Formation of binary solid solutions with other cubic perovskite oxides with superior dielectric properties such as $BaTiO_3$ and $PbTiO_3$[29–34] has also been explored and attempts to chemically modify bismuth ferrites by suitable substitution have targeted the use of $BiCoO_3$, $Ba(Zr_{0.6}Ti_{0.4})O_3$, and $BiMnO_3$, respectively.[35–37] A number of $BiFeO_3$-$BaTiO_3$ (BFO-BTO) solid solution films have been produced using physical and chemical techniques such as pulsed laser deposition,[38] reactive rf sputtering,[39,40] and sol-gel processing.[41] Prior literature suggests that structural crystallographic changes in the resultant solid solution system occur with increasing content of $BaTiO_3$. In $BiFeO_3$-rich solid solution systems, the crystallographic structure is effectively rhombohedral.[42,43] Specifically, in $BiFeO_3$-$BaTiO_3$ solid solutions, rhombohedral symmetry is maintained from 100 to 67 mol % of $BiFeO_3$, after which cubic symmetry predominates down to a level of 7 mol % of $BiFeO_3$. Below that molar value until pure $BaTiO_3$ is achieved, tetragonal symmetry prevails.[44–46] The accompanying changes in lattice parameter, volume of the unit cell, and material density have been previously analyzed.[40]

What is critical to note herein is that these structural transformations of $BiFeO_3$-based binary solid solutions are often correlated with their magnetic as well as electronic properties. For instance, $BiFeO_3$-$BaTiO_3$ has been reported to possess ferromagnetism at room temperature, apart from being both antiferromagnetic and ferroelectric.[47] With increasing concentrations of $BaTiO_3$, the extent of rhombohedral distortion and the degree of ferromagnetic order decrease, such that at the highest concentrations of $BaTiO_3$, the solid solution should exhibit paramagnetic properties.[44,45,48,49] It has also been predicted that the presence of the nonmagnetic $BaTiO_3$ phase could cause a reduction in the strength of the magnetic interaction, thus diminishing the systemic Néel temperature below room temperature.[14]

Nonetheless, in spite of an intense effort directed at creating and probing $BiFeO_3$-based solid solution materials, a fundamental understanding of structure-property correlations in these systems is still lacking. Specifically, insights into the dependence of ferroic ordering behavior and the associated magnetic response on parameters such as crystallinity, size, morphology, purity, and precise chemical composition remain of deep interest. As compared with thin-film multiferroic investigations,[5] less effort has been expended in research associated with the rational synthesis and design of nanostructures of $BiFeO_3$ combined with other perovskite oxides, and, in particular, on the nanoscale preparation of single-crystalline $BiFeO_3$-ABO_3 solid solution structures (including nanocubes) wherein ABO_3 includes the class of perovskites. Our groups have prior experience with analyzing size- and structure-dependent magnetic properties of as-prepared single-crystalline $BiFeO_3$ nanoparticles, polycrystalline $BiFeO_3$ nanotubes, $Bi_2Fe_4O_9$ cubes, and α-Fe_2O_3 rhombohedra.[13,50–53] Herewith, we present the synthesis and characterization of nanoscale substrate-free BFO-BTO structures and a systematic analysis of their magnetic properties as a function of composition.

Powders of BFO-BTO have been previously prepared by a conventional solid-state reaction method involving high-temperature calcination of inorganic precursors pressed into a pellet.[14,46,49,54] In this work, based on previous reported protocols we have utilized to generate magnetic nanostructures,[51,52] we have employed a large scale, facile, and environmentally friendly solid-state reaction using molten salt (i.e., NaCl in the presence of a nonionic surfactant) as our reaction medium as a means of carefully designing a series of single-crystalline BFO-BTO solid solutions possessing controllable composition. In agreement with work cited herein, as generated, purified nanoscale perovskite $(BFO)_x$-$(BTO)_{1-x}$ solid solutions with "x" values of 0.9, 0.8, 0.7, 0.6, and 0.5 have shown an appreciable magnetic response, which is noticeably absent in bulk $BiFeO_3$ (i.e., $x=1$). This assertion has been substantiated from the interpretation of both superconducting quantum interference device (SQUID) and x-ray powder-diffraction measurements. In addition, the electronic structure at the site of the iron and the internal magnetic fields of the solid solutions were recorded by Mössbauer spectroscopy.

II. EXPERIMENTAL

A. Materials preparation

Bismuth (III) acetate (Aldrich, 99.99+%), bismuth (III) oxide (Aldrich, 99.99%), iron (III) oxide (Aldrich, nanoscale powder), barium oxalate (95%, Alfa Aesar), titanium dioxide (Aldrich, anatase, 99.7+%), barium titanate (Aldrich, 99 +%), NP-9 [Aldrich, polyoxyethylene(9)nonylphenyl ether] surfactant, and sodium chloride (Mallinckrodt) were used, as supplied. $BaTiO_3$ itself was chosen as a precursor due to its compatibility and prior use within the context of molten salt reactions.[55] The choice of NP-9 surfactant was governed by its proven versatility in the preparation of various metal oxide systems, its relative nontoxicity, as well as its comparative facility of use.[51,52,55] Hence, herein, a series of $(BFO)_x$-$(BTO)_{1-x}$ solid solution cubes, of varying x, has been prepared using a controlled variation in the molar ratios of Bi, Fe, Ba, and Ti precursors in the experimental procedure. Specifically, stoichiometric amounts of

$[Bi(CH_3COO)_3, \frac{1}{2}Fe_2O_3]:(BaC_2O_4,TiO_2):NaCl:NP\text{-}9$ precursors were mixed in molar ratios of 1:0:20:3, 0.9:0.1:20:3, 0.8:0.2:20:3, 0.7:0.3:20:3, 0.6:0.4:20:3, 0.5:0.5:20:3, and 0:1:20:3 corresponding to $x=1$, 0.9, 0.8, 0.7, 0.6, 0.5, and 0, respectively, in the final products for the corresponding generation of varying concentrations of BFO-BTO solid solutions, containing successively lower amounts of bismuth ferrite. These solid solutions were thoroughly ground in an agate mortar, and subsequently sonicated.

In a typical synthesis of single-crystalline BFO-BTO solid solution cubes, 1, 0.5, 1, and 1 mmol of $Bi(CH_3COO)_3$, Fe_2O_3, BaC_2O_4, and TiO_2, respectively, along with 40 mmol of NaCl, were thoroughly mixed in an agate mortar. The resulting mixture was meticulously stirred for at least 30 min after which 2 ml of NP-9 was subsequently added. Identical procedures were employed for samples containing different molar ratios of initial precursors. The resulting mixture was then placed in a ceramic crucible, inserted into a quartz tube, heated at a ramp rate of 5 °C per min up to an annealing temperature at 820 °C for 3.5 h, and cooled thereafter to room temperature. As-prepared material was subsequently washed several times with distilled water, collected by centrifugation, and dried at 120 °C in a drying oven.

As a means of comparison to these as-prepared samples, a commercial bulk sample of $BaTiO_3$ was used. A bulk $BiFeO_3$ sample was prepared, following the solid-state procedure reported by Achenbach *et al.*[56] in the absence of NaCl and surfactant. Briefly, Bi_2O_3 and Fe_2O_3 combined with a molar ratio of 2:1 were ground thoroughly, and the mixture was annealed at 750 °C for 3 h, followed by air quenching. Residual Bi_2O_3 was removed by a multiple-step nitric acid (17%) leaching process. The resultant sample was washed several times with distilled water and lastly with ethanol. As-obtained samples were ground into a fine powder.

B. Characterization

The dimensions of as-prepared nanocubes were initially characterized using a field-emission scanning electron microscopy (SEM) instrument (Leo 1550), operating at an accelerating voltage of 15 kV and equipped with energy-dispersive x-ray spectroscopy capabilities, as well as with a Hitachi S-4800 at an accelerating voltage of 1.0 kV. Samples for SEM were prepared by dispersing as-prepared nanocubes in ethanol, sonicating for about 2 min, and then depositing the sample onto a silicon wafer, attached to a SEM aluminum stub.

Low-magnification transmission electron microscopy (TEM) images were taken at an accelerating voltage of 80 kV on a FEI Tecnai12 BioTwinG^2 instrument, equipped with an AMT XR-60 charge coupled device digital camera system. High-resolution TEM images were obtained on a JEOL 2010F instrument at accelerating voltages of 200 kV. Specimens for all of these TEM experiments were prepared by dispersing the as-prepared product in ethanol, sonicating for 2 min to ensure adequate dispersion of the nanocubes, and dipping one drop of the solution onto a 300 mesh Cu grid, coated with a lacey carbon film.

To prepare powder x-ray diffraction (XRD) samples, the resulting samples were rendered into slurries in ethanol, sonicated for about 1 min, and then air dried upon deposition onto glass slides. Diffraction patterns were collected using a Scintag diffractometer, operating in the Bragg-Bretano geometry and using Cu *Ka* radiation ($\lambda=1.54$ Å) from $10° \leq 2\theta \leq 80°$ at a scanning rate of 2° in 2θ per minute.

We also performed high-resolution synchrotron x-ray powder diffraction at the X7A beamline at the National Synchrotron Light Source (NSLS). Each powdered sample was loaded into a glass capillary of 0.5 mm diameter, which was then sealed and mounted on the second axis of the diffractometer. A monochromatic beam was obtained using a channel-cut Ge(111) single crystal, and the wavelength of 0.31840(2) Å was calibrated using a CeO_2 standard (SRM 674). A gas-proportional position-sensitive detector (PSD), gated at the Kr-escape peak, was employed for high-resolution ($\Delta d/d \approx 10^{-3}$) powder-diffraction data measurements. The PSD was stepped at 0.25° intervals between 10° and 80° in 2θ with increasing counting times at higher angles. The sample capillary was spun during the measurements for better powder averaging.

Magnetization measurements were obtained using a Magnetic Property Measurement System (MPMS) SQUID magnetometer. Powder samples of BFO-BTO solid solutions were pressed lightly, then loaded into a gel cap, and covered with silica wool. This was held within a uniform drinking straw, which was attached to the sample rod of the MPMS apparatus. Signals generated by measurements of an empty sample holder demonstrated that the holder assembly contributes $<1\%$ to the overall magnetic signal.

Mössbauer spectra were collected using a conventional, constant acceleration transmission Ranger Electronics spectrometer. The γ-ray source consisted of a 30-mCi-^{57}Co in a Rh matrix. The spectrometer was calibrated using a 6 μm iron foil enriched in ^{57}Fe. Isomer shifts are reported relative to metallic iron at room temperature. The experimental data were least square fitted to theoretical spectra using the software package WMOSS by Web Research Co. The analysis assumed a superposition of magnetic and quadrupolar spectra with Lorentzian absorption lines as well as a distribution of magnetic hyperfine fields.

III. RESULTS AND DISCUSSION

A. XRD data: Purity, crystallinity, and phase transformation of $(BFO)_x$-$(BTO)_{1-x}$ samples

The purity and crystallinity of the as-prepared $(BiFeO_3)_x$-$(BaTiO_3)_{1-x}$ solid solution series were examined by powder XRD measurements (Fig. 1). XRD patterns from $(BFO)_x$-$(BTO)_{1-x}$ solid solution samples, with $x=1$, 0.9, 0.8, 0.7, 0.6, 0.5, and 0 are shown in Figs. 1(a)–1(g), respectively. We note that samples (a) and (g) are associated with as-prepared $BiFeO_3$ ($x=1$) and commercial $BaTiO_3$ ($x=0$) powders, respectively. That is, these two latter samples bracket our solid solution series in terms of composition. In effect, diffraction peaks in Fig. 1(a) can be indexed to the rhombohedral structure (space group: $R3c$) of $BiFeO_3$ with lattice constants of $a=b=c=5.63$ Å and $\alpha=\beta=\gamma=59.4°$, which are in good agreement with literature results [i.e., JCPDS (Joint Committee on Powder Diffraction Standards) No. 20-0169].

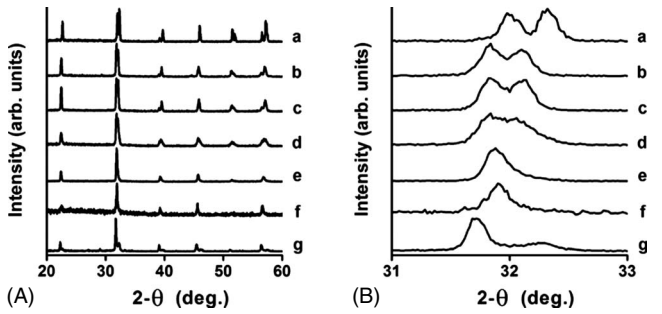

FIG. 1. (A) XRD patterns of (a) $BiFeO_3$ bulk materials (i.e., $x=1$), of $(BiFeO_3)_x$-$(BaTiO_3)_{1-x}$ solid solutions with x values of (b) 0.9, (c) 0.8, (d) 0.7, (e) 0.6, and (f) 0.5, and of (g) $BaTiO_3$ materials (i.e., $x=0$). (B) Expanded view of XRD patterns of $(BiFeO_3)_x$-$(BaTiO_3)_{1-x}$ solid solutions.

Likewise, diffraction peaks in Fig. 1(g) can be indexed to the cubic lattice (space group: $Pm3m$) of $BaTiO_3$, and the calculated lattice constant is $a=4.003$ Å, a value similarly in excellent agreement with the corresponding literature ($a=4.031$ Å, JCPDS No. 31-0714).

Proceeding through our series of pure single-phase solid solutions of metal oxides, the XRD peaks show continuous shifts to lower two-theta values with decreasing x, as expected. In addition, the evolution of the XRD patterns signals successive phase transformations from rhombohedral (when $x=1.0$, 0.9, 0.8, and 0.7) to cubic (when $x=0.6$ and 0.5) and finally, onto tetrahedral (when $x=0$, i.e., pure $BaTiO_3$) phases, as a function of increasing the relative concentration of the titanate constituent (i.e., $BaTiO_3$). Indeed, this structural transition behavior is compatible with literature results for the bulk.[44–46] Moreover, the observed patterns of our collected powders display all of the expected phases emanating from either pure $BiFeO_3$ and/or $BaTiO_3$ structures.

To further detail the precise nature of the structural transition of our as-prepared $(BFO)_x$-$(BTO)_{1-x}$ solid solutions, we have performed high-resolution monochromatic synchrotron x-ray powder diffraction at the X7A beamline at the NSLS. Observed changes in the peak positions are shown in Fig. 2. The diffraction patterns for the Fe-containing component [i.e., $BiFeO_3$, Fig. 2(a)] and the Ti-containing constituent [i.e., $BaTiO_3$, Fig. 2(e)] exhibit signals consistent with as-expected rhombohedral and cubic structures, respectively. Moreover, the diffraction pattern for the $(BFO)_{0.5}$-$(BTO)_{0.5}$ solid solution [Fig. 2(d)] can be ascribed to a perfect cubic structure, thereby confirming the successive phase transition as a function of x. Further analyses based on these data, e.g., peak fittings, structure refinements, and lattice parameters, are currently under investigation.

B. SEM data: Size, shape, and composition of $(BFO)_x$-$(BTO)_{1-x}$ solid solution nanocubes

Figure 3 shows SEM images that reveal the morphologies of as-prepared $(BFO)_x$-$(BTO)_{1-x}$ solid solution nanocubes. It can be observed that these $(BFO)_x$-$(BTO)_{1-x}$ solid solution products, prepared using a molten salt method, mainly consist of discrete cubic structures with relatively smooth surfaces [Figs. 3(A)–3(C)]. Sizes of our as-prepared

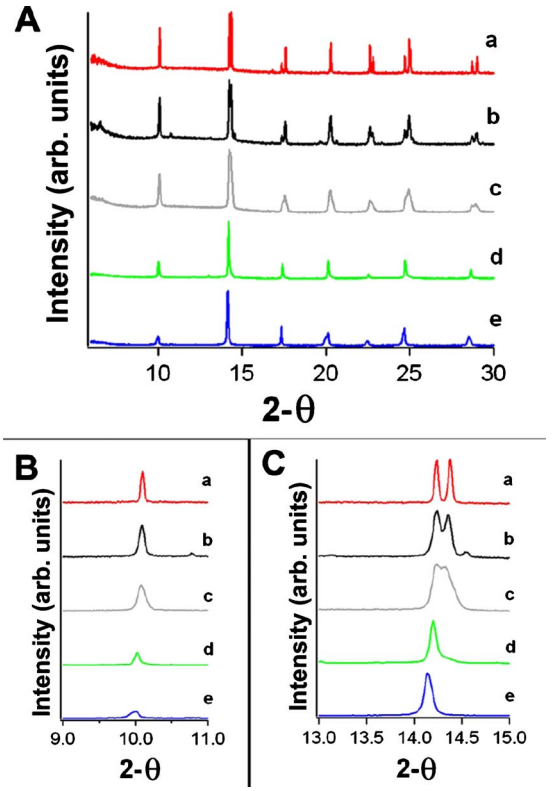

FIG. 2. (Color online) (A) High-resolution synchrotron XRD patterns of (a) $BiFeO_3$ bulk materials (i.e., $x=1$), of $(BiFeO_3)_x$-$(BaTiO_3)_{1-x}$ solid solutions with x values of (b) 0.9, (c) 0.7, (d) 0.5, and of (e) commercial $BaTiO_3$ (i.e., $x=0$). Expanded views of the XRD patterns are shown between (B) 9° and 11° as well as between (C) 13° and 15° to illustrate successive phase transitions with respect to chemical composition in the BFO-BTO solid solution series.

$(BFO)_x$-$(BTO)_{1-x}$ solid solution samples, that had been created with x values of 0.5 (A), 0.7 (B), and 0.9 (C), measured 200 ± 63 nm, 157 ± 48 nm, and 149 ± 79 nm, respectively. We note that SEM images of $(BFO)_x$-$(BTO)_{1-x}$ solid solutions, possessing x values of 0.6 and 0.8, also exhibited similar shapes as compared with those noted in (A)–(C). It can

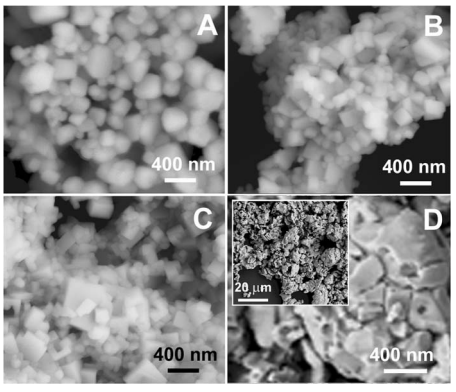

FIG. 3. SEM images of as-prepared $(BiFeO_3)_x$-$(BaTiO_3)_{1-x}$ solid solutions, with x values of (A) 0.5, (B) 0.7, and (C) 0.9, and (D) of bulk $BiFeO_3$ materials, i.e., $x=1$. An inset to (D) illustrates a lower magnification (lower resolution) overview of the image.

also be observed that exposed faces of as-prepared $(BFO)_x$-$(BTO)_{1-x}$ solid solutions are essentially flat, though some of the corners of these structures were slightly truncated.

The morphologies of bulk $BiFeO_3$ products prepared by a solid-state reaction are shown in Fig. 3(D). Although these images clearly show the presence of crystalline particles with smooth faces, it is also evident that these particles are significantly larger with sizes measuring in the range of tens of microns. Moreover, their size distribution is far more polydisperse and associated particle morphologies are also randomized. This observation therefore confirms the effectiveness of using our molten salt method to generate discrete faceted nanostructures of $(BFO)_x$-$(BTO)_{1-x}$ solid solution systems, with control over their chemical composition and morphology.

C. SQUID data: Magnetic properties of $(BFO)_x$-$(BTO)_{1-x}$ solid solution cubes

To investigate the magnetic properties of as-prepared nanoscale $(BFO)_x$-$(BTO)_{1-x}$ solid solutions at room temperature, magnetic measurements (Fig. 4) were performed on these samples as well as on bulk BFO using a MPMS SQUID magnetometer system. The magnetic response observed as a function of the applied field for our as-prepared $(BFO)_x$-$(BTO)_{1-x}$ solid solutions and for bulk $BiFeO_3$ showed noticeably different behavior in terms of hysteresis loop shape. Bulk $BiFeO_3$ (i.e., $x=1$) evinced no hysteretic behavior, as expected, and the accompanying magnetization value (M_s) at 50 kOe was relatively low (~0.34 emu/g at 300 K), as compared with that for the solid solution samples (Table I). By contrast, the magnetic response observed for our as-prepared $(BFO)_x$-$(BTO)_{1-x}$ solid solutions showed appreciable hysteretic behaviors in their curves (Fig. 4 and Table I). The data are consistent with induced ferromagnetism wherein the appearance of hysteresis is presumably due to a canted antiferromagnetic order of Fe-O-Fe chain spins resulting in a weak spontaneous moment.[44] The strength of the response observed at 300 K and an applied magnetic field up to 50 kOe could be described in the following order (in terms of M_s in electromagnetic unit per gram): $(BFO)_{0.8}$-$(BTO)_{0.2}$, $M_s \sim 1.88 > (BFO)_{0.7}$-$(BTO)_{0.3}$, $M_s \sim 1.61 > (BFO)_{0.6}$-$(BTO)_{0.4}$, $M_s \sim 1.49 > (BFO)_{0.9}$-$(BTO)_{0.1}$, $M_s \sim 1.04 \cong (BFO)_{0.5}$-$(BTO)_{0.5}$, $M_s \sim 1.05$.

At 300 K, the $(BFO)_{0.8}$-$(BTO)_{0.2}$ solid solution exhibited the largest magnetic response ($M_s \sim 1.88$ emu/g) as a function of the applied magnetic field among all of the $(BFO)_x$-$(BTO)_{1-x}$ solid solutions. This value was comparable to that observed for previously generated, substrate-free $BiFeO_3$ nanoparticles (~1.55 emu/g) measuring 14 nm in diameter.[13] In effect, the maximum magnetization of our as-prepared $BiFeO_3$ nanoparticles estimated from a linear extrapolation of our results attained values of up to ~1.82 emu/g.[13] Thus, approaches focused on the rational design of $(BFO)_x$-$(BTO)_{1-x}$ solid solutions herein have yielded a slightly higher attainable magnetization. However, we note that this magnetization value generated by incorporation of $BaTiO_3$ into a $BiFeO_3$ matrix is still relatively small for general applicability in memory devices, although the outlook for specific applications at room temperature, involving spintronics, for example, remains highly promising with these nanoscale materials.[13]

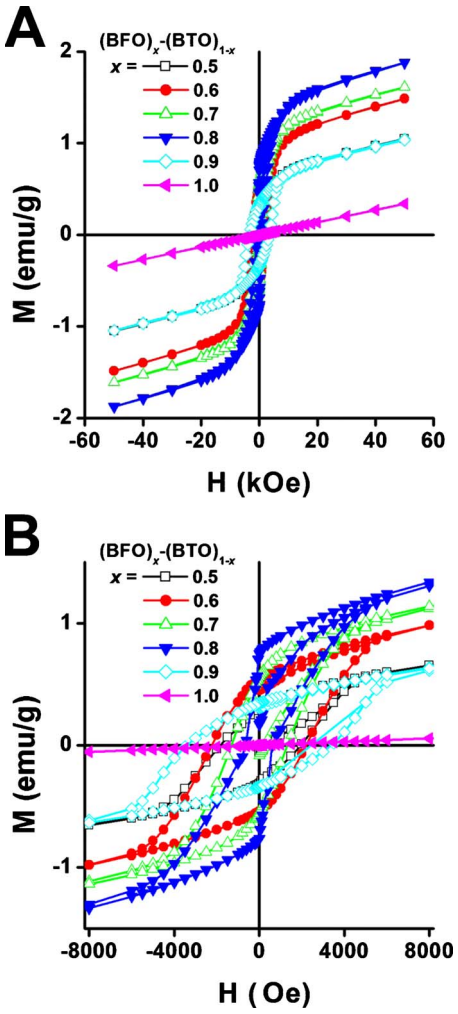

FIG. 4. (Color online) (A) Hysteresis loops at 300 K for as-prepared $(BiFeO_3)_x$-$(BaTiO_3)_{1-x}$ solid solutions with indicated x values. (B) Expanded plots of magnetization at 300 K of as-synthesized $(BiFeO_3)_x$-$(BaTiO_3)_{1-x}$ solid solutions with indicated x values.

To put our measured magnetization value in context, we compared the magnetic values such as remnant magnetization and coercivity of our as-prepared $(BFO)_{0.8}$-$(BTO)_{0.2}$ solid solution nanostructures with that of bulk $(BFO)_{0.8}$-$(BTO)_{0.2}$ solid solution, respectively, which has been previously reported.[21] The remnant magnetization value (M_r: ~0.75 emu/g) measured for our nanostructures is almost an order of magnitude higher than that associated with the literature value (~0.08 emu/g).[21] However, our as-prepared $(BFO)_{0.8}$-$(BTO)_{0.2}$ solid solution nanocubes exhibit relatively lower coercivity (H_c:660 Oe at 300 K) as compared with the measured bulk coercivity (H_c:1000 Oe) for a typical BFO-BTO system.[21] Hence, we believe that the finite-size effect associated with our nanostructured solid solutions plays an important role in enhancing the magnetic

TABLE I. Derived magnetic parameters for $(BiFeO_3)_x$-$(BaTiO_3)_{1-x}$ solid solution cubes as well as for $BiFeO_3$ bulk. M_s is the magnetization observed at $H=50$ kOe. M_r stands for remnant magnetization. The magnetic moments are defined in units of emu/g. H_c represents the derived coercivity.

	M_s at 50 kOe (emu/g)		M_r (emu/g)		H_c (Oe)	
x	300 K	10 K	300 K	10 K	300 K	10 K
0.5	1.05	2.36	0.32	0.46	1840	1300
0.6	1.49	2.61	0.54	0.77	2240	1560
0.7	1.61	2.84	0.56	0.60	1320	910
0.8	1.88	2.87	0.75	0.99	660	480
0.9	1.04	1.42	0.34	0.48	3400	2500
1.0[a]	0.34	0.31				

[a]$BiFeO_3$ bulk shows no spontaneous magnetization.

response of $(BFO)_x$-$(BTO)_{1-x}$ solid solutions. Moreover, the shape control of our solid solution samples (i.e., cubes for our as-prepared samples in this case) may be of special value in possible future device applications.

We note, however, that the recently reported[14] antiferromagnetic behavior of polydispersed randomly shaped $(BFO)_{0.7}$-$(BTO)_{0.3}$ solid solution ceramics maintaining a similar dimensional size (i.e., 200–300 nm) is clearly different from that of our nanocubes herein. This observation further underscores the fact that reported magnetic parameters of $(BFO)_x$-$(BTO)_{1-x}$ solid solution structures are preparation dependent and need further scientific attention and investigation. Reported coercivities at 300 K in the literature for $(BFO)_x$-$(BTO)_{1-x}$ solid solution structures not only deviate from our own data but also vary often significantly among different groups and laboratories. For instance, for $x=0.9$, coercivity values range from ~50 Oe[48] to 1261 Oe[44] while for $x=0.8$, coercivities of ~1000 Oe[21] to 2260 Oe[44] have been reported. For $x=0.75$, figures of ~150 Oe[48] to 1000 Oe[49] have been noted while for $x=0.7$, values of ~0 Oe,[14] 200 Oe,[38] and ~250 Oe[39] have been calculated. Finally, for $x=0.5$, a value of ~0 Oe[21] was reported. Derived magnetic parameters (e.g., M_s, M_r, and H_c) for our as-prepared $(BFO)_x$-$(BTO)_{1-x}$ solid solution nanocubes at 300 K are summarized in Table I.

The magnetic responses observed at 10 K as a function of the applied field for our as-prepared $(BFO)_x$-$(BTO)_{1-x}$ solid solutions and for bulk $BiFeO_3$ are shown in Figs. 5(A) and 5(B). As the nonmagnetic $BaTiO_3$ concentration increases and the composition-dependent crystallographic structure simplifies to a motif possessing high symmetry, the area enclosed by the hysteresis loop decreases, indicating the appearance of a paramagnetic state with weak ferromagnetism. Magnetization measurements on our as-prepared $(BFO)_x$-$(BTO)_{1-x}$ solid solutions at 10 K also exhibited hysteretic behavior with enhanced saturation magnetization values as compared with results at 300 K. To highlight this point, hysteresis loops of a $(BFO)_{0.5}$-$(BTO)_{0.5}$ solid solution at 10 K as well as at 300 K are shown in Fig. 5(C). A comparison between M_s values measured at 10 and 300 K is shown in Fig. 5(D). A peak in the saturation magnetization was observed at a composition range of 80% $BiFeO_3$, in agreement with prior bulk results.[44] Additional derived magnetic parameters (e.g., M_s, M_r, and H_c) at 10 K are summarized in Table I.

As expected, the low-temperature magnetic characteristics show improved values for M_s and M_r for all $(BFO)_x$-$(BTO)_{1-x}$ solid solutions but unexpectedly, the H_c values are smaller at 10 K than at 300 K. In the absence of any other competing interactions, the maximum possible coercivity is given by

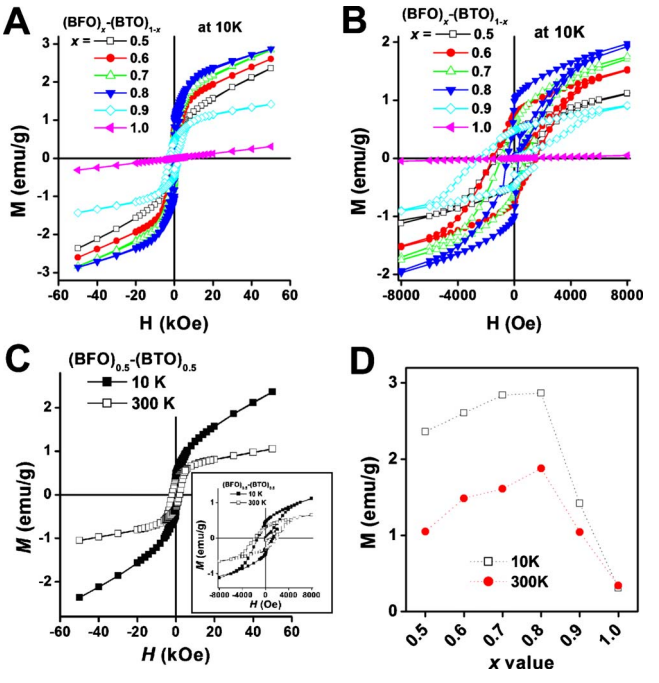

FIG. 5. (Color online) (A) Hysteresis loops at 10 K for as-prepared $(BiFeO_3)_x$-$(BaTiO_3)_{1-x}$ solid solutions with indicated x values. (B) Expanded plots of magnetization at 10 K of as-synthesized $(BiFeO_3)_x$-$(BaTiO_3)_{1-x}$ solid solutions with indicated x values. (C) Corresponding magnetization data for as-prepared $(BiFeO_3)_{0.5}$-$(BaTiO_3)_{0.5}$ solid solution samples at 10 K and 300 K, respectively, are also presented. Inset shows expanded plots of magnetization at 10 K and 300 K, respectively. (D) Spontaneous magnetization values at 10 K and 300 K of as-prepared $(BiFeO_3)_x$-$(BaTiO_3)_{1-x}$ solid solutions at 50 kOe as a function of x values, respectively.

$$H_c = \frac{2K_u}{M_s}, \quad (1)$$

where K_u is the uniaxial magnetic anisotropy of the crystal and M_s is the saturation magnetization.[57] The coercivity is expected to increase with decreasing temperature since the anisotropy decreases much more sharply than does the magnetization with increasing temperature.[58] In ferromagnetic nanostructures with strong demagnetization fields, a reversal of this tendency has been observed if shape anisotropy is present.

In this case,

$$H_c = \frac{2K_u}{M_s} - NM_s, \quad (2)$$

where NM_s is due to shape anisotropy.[59,60] The TEM images of our nanostructures show a preponderance of nanocubes as opposed to nanorod-shaped structures and thus, no major contribution of shape anisotropy would be expected. In addition, the magnetic ordering in our system is antiferromagnetic, wherein the effect of shape anisotropy is greatly diminished due to smaller demagnetization fields. That leaves the possibility of magnetoelectric coupling as a potential candidate to produce a competing interaction. In the presence of magnetoelectric coupling, the uniaxial magnetic anisotropy energy is modified according to Eq. (3),

$$K_u' = K_u - \chi^{\perp}(\beta P_z)^2/2, \quad (3)$$

where β is the homogeneous magnetoelectric coefficient that relates the Dzyaloshinsky-Moria magnetic field and the spontaneous polarization P_z, and $\chi^{\perp}$ is the magnetic susceptibility in the direction perpendicular to the antiferromagnetic vector.[12,23]

Thus, the reduction in coercivity at low temperature as compared with the room-temperature value for all the compositions studied could possibly be explained by the presence of magnetoelectric coupling in these systems. A similar reduction in coercivity at low temperatures has been previously reported for $BiFeO_3$-$PbTiO_3$-based ceramics.[23] Direct evidence for a strong, intrinsic, multiferroic magnetoelectric coupling has also been reported for bulk $(BFO)_{0.9}$-$(BTO)_{0.1}$, wherein a linear magnetoelectric coupling was noted in the relevant data.[7]

D. Mössbauer studies of $(BFO)_x$-$(BTO)_{1-x}$ solid solution cubes

The electronic and magnetic properties of the BFO-BTO solid solution nanostructures were also systematically investigated by Mössbauer spectroscopy. Figure 6 shows the Mössbauer spectra obtained for $(BFO)_x$-$(BTO)_{1-x}$, where $0.5 \leq x \leq 1$. The solid lines give least-square fits of the experimental spectra to theoretical spectra, assuming Lorentzian absorption line shapes and a distribution of magnetic hyperfine fields. Figure 6(A) shows the Mössbauer spectrum of bulk bismuth ferrite. The magnetic spectral signature observed corresponds to high spin ferric ions in the $BiFeO_3$ crystal lattice. The characteristic asymmetry in the spectra of the bulk has been previously reported[61] and has been reproduced by our bulk material [Fig. 6(A)]. The observed asymmetry has been attributed to the superposition of two magnetic subsites due to Fe^{3+} in two different crystallographic environments that differ primarily in the size of the electric-field gradient.[61] Best fits of our experimental data to theoretical spectra give values for the isomer shift of $\delta_1 = 0.39$ mm/s and $\delta_2 = 0.38$ mm/s; magnetic hyperfine field of $H_{hf1} = 494$ kOe and $H_{hf2} = 498$ kOe; and quadrupolar perturbation of $\varepsilon_1 = -0.10$ mm/s and $\varepsilon_2 = 0.34$ mm/s for the two subsites.

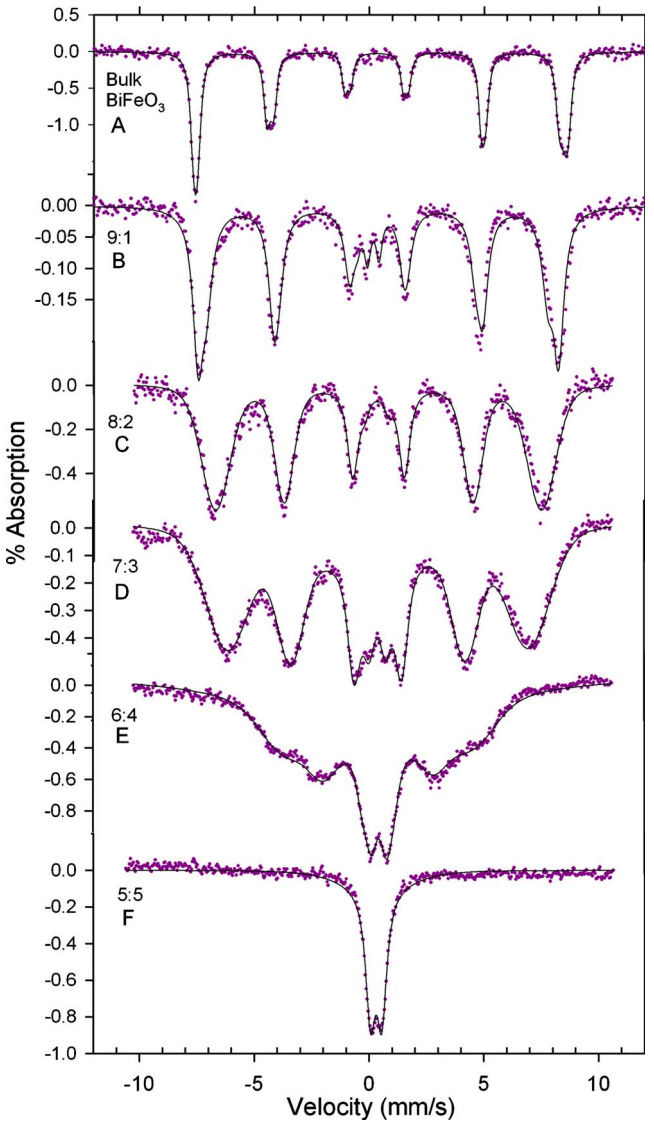

FIG. 6. (Color online) Mössbauer spectra for $(BiFeO_3)_x$-$(BaTiO_3)_{1-x}$ nanocubes at room temperature; (A) $x=1$, (B) $x=0.9$, (C) $x=0.8$, (D) $x=0.7$, (E) $x=0.6$, and (F) $x=0.5$. The solid lines are theoretical fits to the experimental points, assuming a superposition of quadrupolar and magnetic subspectra with Lorentzian absorption lines, including a distribution of magnetic hyperfine fields (see text).

With increasing content of $BaTiO_3$ in the composition of the solid solution, the resolution of the two subsites is lost as the spectra become broadened due to the nature of disorder in the superexchange magnetic interaction paths resulting from the random substitution of Fe^{3+} ions by nonmagnetic Ti^{4+} ions within the structure of $BiFeO_3$. Concomitantly, the

overall splitting of the outer magnetic absorption lines which measures the average effective magnetic hyperfine field at the nucleus decreases, reflecting the weakening of the inherent strength of the magnetic interactions. Specifically, from Figs. 6(B)–6(E), we obtain H_{hf} values of 477 kOe for $x=0.9$, 439 kOe for $x=0.8$, 406 kOe for $x=0.7$, and 254 kOe for $x=0.6$, respectively.

The overall spectral characteristics indicate the formation of single solid solution phases and a gradual magnetic phase transformation from a well-ordered spin structure for pure $BiFeO_3$ to an increasingly spin disordered magnetic phase. Simultaneously, the local magnetic anisotropy energy diminishes, resulting in spin fluctuations producing the collapsed quadrupolar spectral subcomponents superimposed onto the magnetic spectra and a broad diffuse background. These observations are consistent with the reduction in the Néel temperature of the material with decreasing x. Eventually, the system with composition, $x=0.5$, exhibits only a broadened quadrupolar signature consistent with a paramagnetic phase ($\delta=0.31$ mm/s and $\Delta E_Q=0.50$ mm/s), similar to that obtained not only for as-deposited $(BiFeO_3)_{0.5}$-$(PbTiO_3)_{0.5}$ films[39] but also for bulk $BiFeO_3$ above its Néel temperature,[61] indicating that the Néel temperature for the $x=0.5$ composition is below room temperature.

An interesting and significant observation can be made when one compares the Mössbauer data with the magnetization results corresponding to the $x=0.5$ composition. The observation of hysteresis in the magnetization study indicates a magnetically ordered phase while the collapsed quadrupolar Mössbauer spectrum suggests a paramagnetic phase. Our previous studies of the magnetic properties of $BiFeO_3$ as a function of particle size[13] indicate that superparamagnetic relaxation appears in particles measuring ~50 nm in size and smaller. Herein, our particles measuring ~200 nm in diameter are not close to the superparamagnetic regime. Therefore, the collapse of the magnetic structure in the Mössbauer spectra can only be associated with the attainment of a critical temperature, such as the Néel temperature, as discussed above. Thus, the discrepancy between the magnetization measurements and the Mössbauer data cannot be explained away in terms of merely blocking temperature differences associated with superparamagnetic relaxation between the two techniques, since, in any case, higher blocking temperatures would have been expected for Mössbauer as opposed to SQUID measurements.[62]

The only real difference in sample treatment is that the sample used in the magnetization study was exposed, by the very nature of the measurement, to an external magnetic field, whereas the sample used in the Mössbauer study was never subjected to a magnetic field. We propose that the observed field-induced magnetic ordering, implied by the coercivity of the $x=0.5$ composition, may be due to magnetostriction effects that can induce electrical polarization in the presence of the externally applied magnetic field via the magnetoelectric coupling. Supporting evidence for such a hypothesis was sought in the initial magnetization curve of the $x=0.5$ composition, shown in Fig. 7. At small applied fields, the magnetization increases linearly with the field, consistent with a paramagnetic phase. Close examination of the linear part of the curve (see inset) indicates a sharp discontinuity in the slope at ~2300 Oe of applied field. The initial susceptibility has a magnitude of 0.976×10^{-4} emu/g per Oe and increases discontinuously to 2.19×10^{-4} emu/g per Oe above an applied field of 2300 Oe, before the curve starts to bend above ~4000 Oe. We propose that this observation may be evidence of a field-induced displacive phase transition, due to the presence of a strong magnetoelectric or magnetoelastic coupling, resulting in the appearance of a new phase with a Néel temperature above room temperature, as indicated by its hysteric behavior at room temperature. Of relevance to our assertion are recent reports on single-crystalline $BiFeO_3$ of the coexistence of large electric polarization and magnetic order,[63] the observation of an electric-field-induced spin-flop phase transition,[64] evidence of strong coupling between magnetic and electrical order parameters at the nanoscale,[65] and the presence of elastic and electrical anomalies.[66]

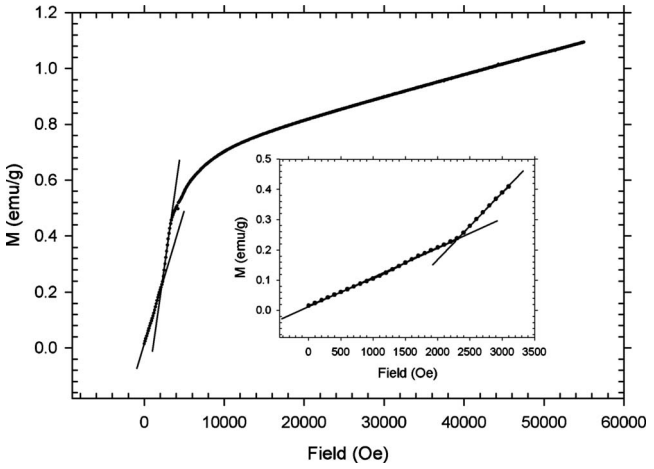

FIG. 7. Initial magnetization curve for $(BiFeO_3)_{0.5}$-$(BaTiO_3)_{0.5}$ at room temperature. Inset clearly shows a sharp discontinuity in the magnetic susceptibility at an applied field of ~2300 Oe (see text).

IV. CONCLUSIONS

Employing molten salt methodology, we have been able to generate highly pure single-crystalline nanocubes of $(BFO)_x$-$(BTO)_{1-x}$, in the form of single-phased solid solutions with x values ranging from 1.0, 0.9, 0.8, 0.7, 0.6, 0.5, to 0. We do not observe any evidence for decomposition of our solid solutions into either distinctive domains or independent phases. The combination of Mössbauer and SQUID measurements has allowed us to systematically probe both the intrinsic and extrinsic magnetic properties of these systems. Our experimental results indicate that the latent magnetization locked up in the spiral spin structure is released at the introduction of even a very small amount of $BaTiO_3$ as evinced by the magnetic properties associated with the composition of $x=0.9$. Furthermore, two experimental observations, namely, the reduction in coercivity at low temperature and the transformation from a paramagnetic to an ordered state for the $x=0.5$ composition upon the application of an external magnetic field, point to the possible presence of magne-

toelectric or magnetoelastic coupling. Hence, the BFO-BTO solid solution system has provided us with fundamental information regarding interactions between the magnetic and electric properties in ferroelectric nanomagnets, which can be further generalized to nanoscale functional materials with a wide range of chemical compositions and structures with promising potential in spintronics applications.[67]

ACKNOWLEDGMENTS

We acknowledge the U.S. Department of Energy (Grant No. DE-AC02-98CH10886) for support of a lot of the magnetic and characterization (excluding the Mössbauer work) studies. S.S.W. also thanks the National Science Foundation (CAREER Award No. DMR-0348239) and the Alfred P. Sloan Foundation for PI and student support as well as for the synthesis studies. G.C.P. thanks the National Science Foundation for overall support under Grant No. DMR-0604049. Moreover, we are grateful to D. Wang (Boston College) as well as to S. van Horn and J. Quinn (SUNY Stony Brook) for their assistance with electron microscopy. Y. Lee thanks support by the Global Research Lab Program of the National Research Foundation of the Korean Government. Research carried out in part at the NSLS at Brookhaven National Laboratory is supported by the U.S. Department of Energy, Office of Basic Energy Sciences.

*Present address: NEAT ORU and Peter A. Rock Thermochemistry Laboratory, University of California at Davis, One Shields Avenue, Davis, California 95616.

†Authors to whom correspondence should be addressed; gcp@villanova.edu and sswong@notes.cc.sunysb.edu

‡Present address: Department of Chemistry and Biochemistry, University of Texas at Austin, 1 University Station, Austin, Texas 78712.

[1] W. Eerenstein, N. D. Mathur, and J. F. Scott, Nature (London) **442**, 759 (2006).
[2] R. E. Cohen, Nature (London) **358**, 136 (1992).
[3] N. A. Hill, J. Phys. Chem. B **104**, 6694 (2000).
[4] P. Fischer, M. Polomska, I. Sosnowska, and M. Szymanski, J. Phys. C **13**, 1931 (1980).
[5] R. Ramesh and N. A. Spaldin, Nature Mater. **6**, 21 (2007).
[6] S. W. Cheong and M. Mostovoy, Nature Mater. **6**, 13 (2007).
[7] A. Singh, V. Pandey, R. K. Kotnala, and D. Pandey, Phys. Rev. Lett. **101**, 247602 (2008).
[8] I. Sosnowska, T. Peterlin-Neumaier, and E. Steichele, J. Phys. C **15**, 4835 (1982).
[9] I. Sosnowska, M. Loewenhaupt, W. I. F. David, and R. M. Ibberson, Physica B **180-181**, 117 (1992).
[10] Yu F. Popov, A. M. Kadomtseva, G. P. Vorob'ev, and A. K. Zvezdin, Ferroelectrics **162**, 135 (1994).
[11] A. M. Kadomtseva, A. K. Zvezdin, Y. F. Popov, A. P. Pyatakov, and G. P. Vorob'ev, JETP Lett. **79**, 571 (2004).
[12] B. Ruette, S. Zvyagin, A. P. Pyatakov, A. Bush, J. F. Li, V. I. Belotelov, A. K. Zvezdin, and D. Viehland, Phys. Rev. B **69**, 064114 (2004).
[13] T.-J. Park, G. C. Papaefthymiou, A. J. Viescas, A. R. Moodenbaugh, and S. S. Wong, Nano Lett. **7**, 766 (2007).
[14] M. T. Buscaglia, L. Mitoseriu, V. Buscaglia, I. Pallecchi, M. Viviani, P. Nanni, and A. S. Siri, J. Eur. Ceram. Soc. **26**, 3027 (2006).
[15] J. Wang, J. B. Neaton, H. Zheng, V. Nagarajan, S. B. Ogale, B. Liu, D. Viehland, V. Vaithyanathan, D. G. Schlom, U. V. Waghmare, N. A. Spaldin, K. M. Rabe, M. Wuttig, and R. Ramesh, Science **299**, 1719 (2003).
[16] S.-T. Zhang, Y. Zhang, M.-H. Lu, C.-L. Du, Y.-F. Chen, Z.-G. Liu, Y.-Y. Zhu, N.-B. Ming, and X. Q. Pan, Appl. Phys. Lett. **88**, 162901 (2006).
[17] G. L. Yuan, S. W. Or, J. M. Liu, and Z. G. Liu, Appl. Phys. Lett. **89**, 052905 (2006).
[18] G. L. Yuan and S. W. Or, J. Appl. Phys. **100**, 024109 (2006).
[19] V. R. Palkar, D. C. Kundaliya, S. K. Malik, and S. Bhattacharya, Phys. Rev. B **69**, 212102 (2004).
[20] D. H. Wang, W. C. Goh, M. Ning, and C. K. Ong, Appl. Phys. Lett. **88**, 212907 (2006).
[21] J. S. Kim, C. I. Cheon, C. H. Lee, and P. W. Jang, J. Appl. Phys. **96**, 468 (2004).
[22] J. S. Kim, C. I. Cheon, Y. N. Choi, and P. W. Jang, J. Appl. Phys. **93**, 9263 (2003).
[23] N. Wang, J. Cheng, A. Pyatakov, A. K. Zvezdin, J. F. Li, L. E. Cross, and D. Viehland, Phys. Rev. B **72**, 104434 (2005).
[24] Y.-H. Lee, J.-M. Wu, and C.-H. Lai, Appl. Phys. Lett. **88**, 042903 (2006).
[25] F. Gao, C. Cai, Y. Wang, S. Dong, X. Y. Qiu, G. L. Yuan, Z. G. Liu, and J.-M. Liu, J. Appl. Phys. **99**, 094105 (2006).
[26] J. S. Kim, C. I. Cheon, H.-J. Kang, and P. W. Jang, J. Eur. Ceram. Soc. **27**, 3951 (2007).
[27] J. Cheng, S. Yu, J. Chen, Z. Meng, and L. Eric Cross, Appl. Phys. Lett. **89**, 122911 (2006).
[28] V. A. Khomchenko, D. A. Kiselev, J. M. Vieira, L. Jian, A. L. Kholkin, A. M. L. Lopes, Y. G. Pogorelov, J. P. Araujo, and M. Maglione, J. Appl. Phys. **103**, 024105 (2008).
[29] A. B. Kounga Njiwa, E. Aulbach, J. Rödel, S. L. Turner, T. P. Comyn, and A. J. Bell, J. Am. Ceram. Soc. **89**, 1761 (2006).
[30] W. M. Zhu and Z.-G. Ye, Ceram. Int. **30**, 1435 (2004).
[31] D. I. Woodward, I. M. Reaney, R. E. Eitel, and C. A. Randall, J. Appl. Phys. **94**, 3313 (2003).
[32] T. Kanai, S. Ohkoshi, A. Nakajima, T. Watanabe, and K. Hashimoto, Adv. Mater. **13**, 487 (2001).
[33] L. Hongri, L. Zuli, L. Qing, and Y. Kailun, J. Phys. D **39**, 1022 (2006).
[34] P. Yang, K. M. Kim, Y.-G. Joh, D. H. Kim, J.-Y. Lee, J. Zhu, and H. Y. Lee, J. Appl. Phys. **105**, 061618 (2009).
[35] M. Azuma, H. Kanda, A. A. Belik, Y. Shimakawa, and M. Takano, J. Magn. Magn. Mater. **310**, 1177 (2007).
[36] R. N. P. Choudhary, K. Perez, P. Bhattacharya, and R. S. Katiyar, Mater. Chem. Phys. **105**, 286 (2007).
[37] S. Yasui, K. Nishida, H. Naganuma, S. Okamura, T. Iijima, and H. Funakubo, Jpn. J. Appl. Phys., Part 1 **46**, 6948 (2007).
[38] K. Ueda, H. Tabata, and T. Kawai, Appl. Phys. Lett. **75**, 555 (1999).

[39] T. Fujii, S. Jinzenji, and Y. Asahara, J. Appl. Phys. **64**, 5434 (1988).
[40] T. Fujii, S. Shimizu, A. Kajima, and T. Miyama, J. Magn. Magn. Mater. **54-57**, 1303 (1986).
[41] R. E. Melgarejo, M. S. Tomar, R. Guzman, and S. P. Singh, Ferroelectrics **324**, 101 (2005).
[42] R. T. Smith, G. D. Achenbach, R. Gerson, and W. J. James, J. Appl. Phys. **39**, 70 (1968).
[43] C. Michel, J.-M. Moreau, G. D. Achenbach, R. Gerson, and W. J. James, Solid State Commun. **7**, 701 (1969).
[44] M. M. Kumar, S. Srinath, G. S. Kumar, and S. V. Suryanarayana, J. Magn. Magn. Mater. **188**, 203 (1998).
[45] M. M. Kumar, A. Srinivas, and S. V. Suryanarayana, J. Appl. Phys. **87**, 855 (2000).
[46] I. H. Ismailzade, R. M. Ismailov, A. I. Alekberov, and F. M. Salaev, Phys. Status Solidi A **68**, K81 (1980).
[47] A. I. Kalshinskii, V. I. Cherchernikov, and Y. N. Venevtsev, Sov. Phys. Solid State **6**, 375 (1964).
[48] M. M. Kumar, A. Srinivas, G. S. Kumar, and S. V. Suryanarayana, J. Phys.: Condens. Matter **11**, 8131 (1999).
[49] Y. Horibe, M. Nakayama, Y. Hosokoshi, T. Asaka, Y. Matsui, T. Asada, Y. Koyama, and S. Mori, Jpn. J. Appl. Phys., Part 1 **44**, 7148 (2005).
[50] T.-J. Park, Y. Mao, and S. S. Wong, Chem. Commun. (Cambridge) **2004**, 2708.
[51] T.-J. Park and S. S. Wong, Chem. Mater. **18**, 5289 (2006).
[52] T.-J. Park, G. C. Papaefthymiou, A. R. Moodenbaugh, Y. Mao, and S. S. Wong, J. Mater. Chem. **15**, 2099 (2005).
[53] T.-J. Park, S. Sambasivan, D. A. Fischer, W.-S. Yoon, J. A. Misewich, and S. S. Wong, J. Phys. Chem. C **112**, 10359 (2008).
[54] S. O. Leontsev and R. E. Eitel, J. Am. Ceram. Soc. **92**, 2957 (2009).
[55] Y. Mao, S. Banerjee, and S. S. Wong, J. Am. Chem. Soc. **125**, 15718 (2003).
[56] G. D. Achenbach, W. J. James, and R. Gerson, J. Am. Ceram. Soc. **50**, 437 (1967).
[57] A. H. Morrish, *The Physical Principles of Magnetism* (IEEE Press, Piscataway, 2001).
[58] R. C. O'Handley, *Modern Magnetic Materials* (Wiley, New York, 2000).
[59] N. A. Frey, R. Heindl, S. Srinath, H. Srikanth, and N. J. Dudney, Mater. Res. Bull. **40**, 1286 (2005).
[60] O. Kubo, T. Ido, and H. Yokoyama, IEEE Trans. Magn. **MAG-18**, 1122 (1982).
[61] C. Blaauw, and F. van der Woude, J. Phys. C **6**, 1422 (1973).
[62] G. Xiao, S. H. Liou, A. Levy, J. N. Taylor, and C. L. Chien, Phys. Rev. B **34**, 7573 (1986).
[63] D. Lebeugle, D. Colson, A. Forget, M. Viret, P. Bonville, J. F. Marucco, and S. Fusil, Phys. Rev. B **76**, 024116 (2007).
[64] D. Lebeugle, D. Colson, A. Forget, M. Viret, A. M. Bataille, and A. Goukasov, Phys. Rev. Lett. **100**, 227602 (2008).
[65] R. Mazumder, P. S. Devi, D. Bhattacharya, P. Choudhury, A. Sen, and M. Raja, Appl. Phys. Lett. **91**, 062510 (2007).
[66] S. A. T. Redfern, C. Wang, J. W. Hong, G. Catalan, and J. F. Scott, J. Phys.: Condens. Matter **20**, 452205 (2008).
[67] H. Béa, M. Gajek, M. Bibes, and A. Barthélémy, J. Phys.: Condens. Matter **20**, 434221 (2008).